



Article

Binder-Free Construction of a Methanol Tolerant Pt/TiO₂/Carbon Paper Anode by Atomic Layer Deposition

Gergő Ballai¹, Tamás Gyenes¹, Henrik Haspel², Livia Vásárhelyi¹ , Imre Szenti¹, Dániel Sebők¹, Zoltán Kónya^{1,3}  and Ákos Kukovecz^{1,*}

¹ Department of Applied and Environmental Chemistry, University of Szeged, Rerrich Béla tér 1, H-6720 Szeged, Hungary; ballai.gergo@gmail.com (G.B.); gyenestomi@indamail.hu (T.G.); vasarhelyil@hotmail.com (L.V.); szentiimre@gmail.com (I.S.); daniel_sebok@yahoo.com (D.S.); konya@chem.u-szeged.hu (Z.K.)

² KAUST Catalysis Center, Advanced Catalytic Materials, King Abdullah University of Science and Technology, Thuwal 23955, Saudi Arabia; henrik.haspel@kaust.edu.sa

³ MTA-SZTE Reaction Kinetics and Surface Chemistry Research Group, Rerrich Béla tér 1, H-6720 Szeged, Hungary

* Correspondence: kakos@chem.u-szeged.hu; Tel.: +36-62-544-620

Abstract: Direct liquid fuel cells are very appealing alternatives for fighting climate change, particularly in the field of personal mobility solutions. This is especially true for direct methanol fuel cells (DMFCs) that use and burn safe fuels that are readily available from sustainable sources using well-established C₁ chemistry. However, DMFCs also have some serious competitive disadvantages, like the high cost of the noble metal catalysts, the difficulties of the catalyst application, and the poisoning of the catalyst due to carbon monoxide formation. Here we demonstrate that depositing platinum on TiO₂ by atomic layer deposition (ALD) is an easy, reproducible method for the synthesis of TiO₂-supported platinum catalyst for methanol oxidation with superior anti-poisoning properties.

Keywords: methanol oxidation reaction; fuel cell; atomic layer deposition; anode; TiO₂



Citation: Ballai, G.; Gyenes, T.; Haspel, H.; Vásárhelyi, L.; Szenti, I.; Sebők, D.; Kónya, Z.; Kukovecz, Á. Binder-Free Construction of a Methanol Tolerant Pt/TiO₂/Carbon Paper Anode by Atomic Layer Deposition. *Catalysts* **2021**, *11*, 154. <https://doi.org/10.3390/catal11020154>

Academic Editor: Vincenzo Baglio

Received: 30 December 2020

Accepted: 19 January 2021

Published: 22 January 2021

Publisher's Note: MDPI stays neutral with regard to jurisdictional claims in published maps and institutional affiliations.



Copyright: © 2021 by the authors. Licensee MDPI, Basel, Switzerland. This article is an open access article distributed under the terms and conditions of the Creative Commons Attribution (CC BY) license (<https://creativecommons.org/licenses/by/4.0/>).

1. Introduction

Polymer electrolyte fuel cells (PEFCs) enjoy increasing scientific attention today due to their low working temperature, high power density, and compact size. This is especially true for direct liquid fuel cells (DLFCs) that can be used with various fuels. Alcohols such as methanol, ethanol, and ethylene glycol, acids such as formic acid, and other materials such as hydrazine or sodium borohydride are all good choices to substitute the most common fuel, hydrogen, due to their superior storage, transfer, and refill characteristics [1]. Methanol is the most widely used liquid fuel for direct liquid fuel cells.

The most typical catalysts in DLFCs today are platinum and platinum-group metals (e.g., palladium, iridium, rhodium, ruthenium) even though it would be desirable to reduce their utilization due to their high price and the negative environmental impact linked to their mining operations [2]. These shortcomings are outweighed by the excellent electrocatalytic properties of platinum. It is the most often used catalyst for both the cathodic side as the oxygen reduction reaction (ORR) catalyst, and the anodic side as the hydrogen oxidation reaction (HOR) or methanol oxidation reaction (MOR) catalyst in fuel cells. In the latter process, carbon monoxide forms as an intermediate that can have serious negative effects on the performance of the catalyst due to strong CO–Pt interactions. The most common solution to this problem is to use platinum alloys such as platinum-ruthenium [3], platinum-palladium [4], or platinum-cobalt [5], where the second metal catalyses CO oxidation either by forming adsorbed OH (OH_{ads}) species or by modifying the platinum electronic structure. The OH_{ads} species react with the surface CO to produce CO₂ and thus make additional active sites available [6].

Transition metal oxides, including titanium oxides, are widely used as catalyst support materials due to their high specific surface area and excellent chemical stability. In the MOR, metal oxides also help the oxidation of carbon monoxide and reduce anode catalyst poisoning. One of the main setbacks of oxides is their low electrical conductivity, especially compared to other supporting materials used in fuel cells, such as carbon structures or metal foams [7–10].

Wet chemical methods (e.g., chemical reduction, polyol, or wet impregnation) are extensively used in both laboratory and industrial practices for catalyst synthesis [11,12]. However, synthesizing the catalyst in the liquid phase and subsequently spray-coating it onto the gas diffusion layer (GDL) surface has serious downsides. These traditional preparation methods are complicated to automatize, especially on the laboratory scale. Homogeneous surface coverage of well-distributed nanoparticles is difficult to obtain [13]. Furthermore, the as-synthesised nanoparticles require a binding agent to hold the nanoparticles in the catalyst layer of the gas diffusion electrode (GDE). In proton exchange membrane fuel cells such as direct liquid fuel cells, Nafion[®] solution has a dual purpose: it is used as an ionomer and a binding agent at the same time. However, excess Nafion[®] has a detrimental effect on fuel cell performance as it deteriorates active site accessibility during operation [14,15]. Therefore, reducing or even eliminating binder use is considered to be beneficial [16]. Consequently, developing methods for the direct synthesis of catalysts on the GDL surface without using any binding agent is a very important contemporary research topic.

Atomic layer deposition (ALD) is a promising technology to directly synthesize nanometre-thick layers or nanosized particles of metals, oxides, nitrides, sulphides, etc. directly on the GDL surface. ALD makes use of the surface reaction of gas-phase precursors to deposit thin films of homogeneous thickness or evenly distributed nanostructures with controllable size and loading. The difference in the surface energy of the substrate and the free energy of the material to be synthesised define whether nanoparticles or layers are formed. When the former is lower, the given material cannot wet the substrate surface, resulting in the formation of nanoclusters or particles. The surface energy of platinum ($\sim 2.5 \text{ J m}^{-2}$) is higher than that of most substrates, hence Pt mostly forms nanoparticles. Metal oxides such as titania have lower surface energy (e.g., anatase: $0.43\text{--}1.61 \text{ J m}^{-2}$, depending on the crystal plane [17]), which in turn favours solid layer formation [18]. Figure 1 illustrates the operation principle of ALD. One ALD cycle typically consists of an exposure of two precursors separated by inert gas purging. Once the first precursor is adsorbed on the substrate surface (B), the non-adsorbed molecules are flushed from the chamber in the purging step (C). The desired material is then formed as the surface is exposed to the second precursor (D). Excess precursors and by-products (CO_2 , H_2O , etc.) are purged in the final step (E). The thickness of the layer or the size of the particle can be controlled by repeating the cycle over and over (F).

Recently ALD has shown great promise in the synthesis of various noble metal catalysts/electrocatalysts for applications such as selective hydrogenation [19], oxidative dehydrogenation [20], water splitting, or for catalysis in fuel cells [18,21,22].

In this work, we suggest a novel synthesis approach to prepare a Pt/TiO₂ fuel cell anode without using any binder or pre-prepared nanoparticle source. Both the TiO₂ layer and the platinum nanoparticles are synthesised directly by atomic layer deposition on carbon paper, and the performance of the ALD-derived electrodes is compared with a reference Pt/carbon paper structure obtained using the conventional polyol synthesis. The new approach eliminates the known issues related to the use of binders and makes it possible to compare the properties of the electrodes without the inherent complications of working with externally obtained nanoparticles. A collateral benefit is that the high degree of ALD automation also promises excellent electrode repeatability.

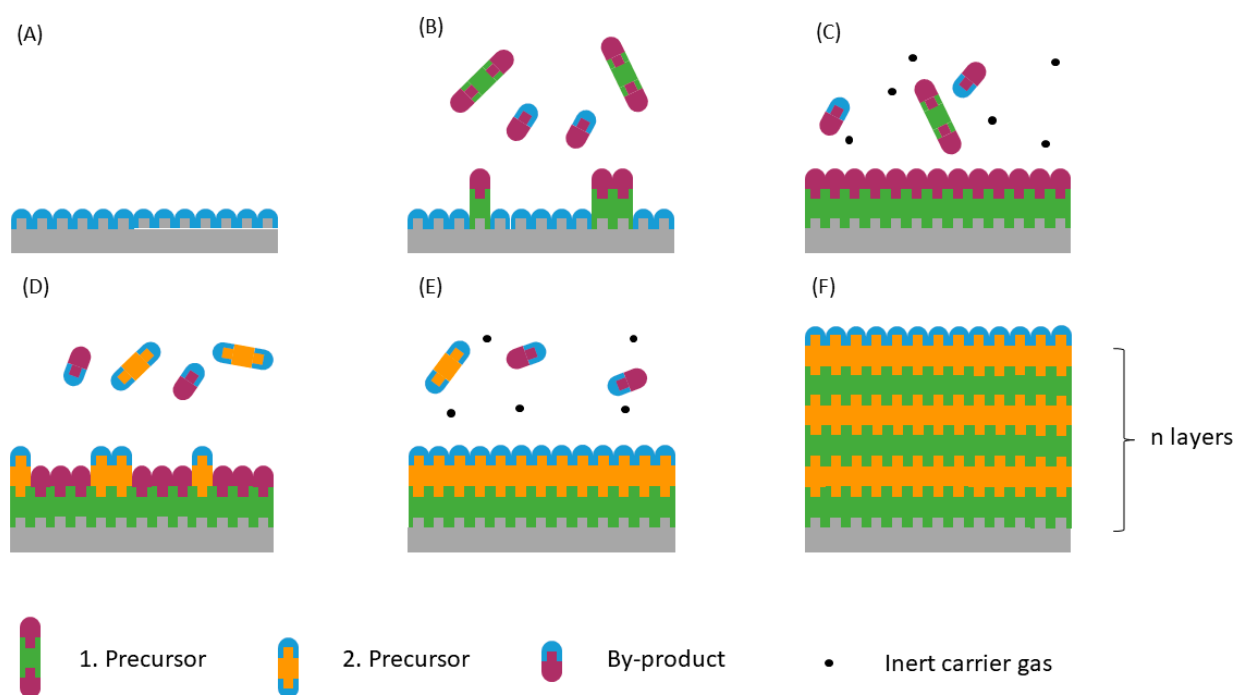


Figure 1. The principle of operation of the atomic layer deposition technique. The substrate before the deposition (A), exposure of the first precursor (B), first purging step (C), exposure of the second precursor (D), second purging step (E), and the formed layer or nanoparticle after n cycles (F).

2. Results and Discussion

2.1. Morphology

The morphology of the ALD-prepared composites was investigated by transmission electron microscopy. As can be seen in Figure 2a,c, platinum nanoparticles were distributed evenly on the surface of the carbon support, while fewer nanoparticles were formed in the titanium-dioxide-containing gas diffusion electrode. This agrees well with the weight measurement, where a significantly lower loading was found in the case of the titania-containing electrode. The average particle sizes were 3.2 nm and 2.4 nm in the 20 ALD cycles of platinum (20c Pt) and 25 ALD cycles of titanate and 20 ALD cycles of platinum (25c TiO₂ + 20c Pt) catalysts, respectively. The difference in particle size could be attributed to the difference of the surface energy, and consequently, the wettability of the carbon and TiO₂-covered carbon supports. The smaller particle size implies higher surface area, which in turn means more active sites for methanol oxidation. Although Frelink et al. reported decreasing Pt catalytic activity with decreasing particle size under 4.5 nm [23], we found higher mass activity with smaller nanoparticles on titanate-covered carbon paper. In the top-right corner of Figure 2, a higher-magnification image can be seen where the lattice distances corresponding to the (111) Miller index plane of platinum are indicated. In Supplementary Materials Figure S3a the transmission electron microscopic images of the polyol-synthesized catalysts are demonstrated. It can be seen that the as-prepared platinum nanoparticles are slightly larger—4.4 nm on average.

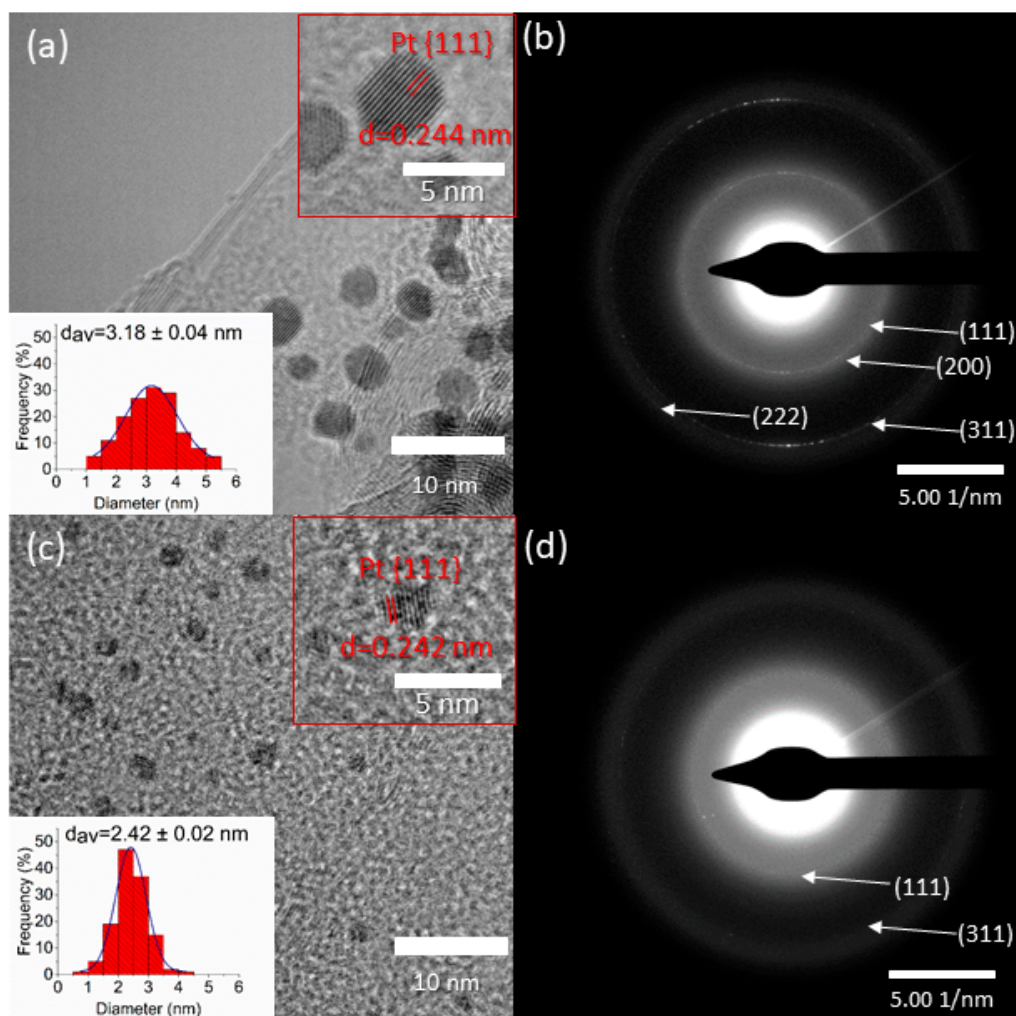


Figure 2. TEM images (a,c) and electron diffractograms (b,d) of the atomic layer deposition (ALD)-synthesised 20c Pt (a,b) and 25c TiO₂ + 20c Pt (c,d) catalysts.

In the electron diffractograms (Figure 2b,d), several Debye–Scherrer rings were identified: the reflections in Figure 2b correspond to the (111), (200), (311), and (222) lattice planes of platinum. In Figure 2d only two rings can be identified due to the smaller amount of the smaller platinum nanoparticles. These rings can be assigned to the (111) and (311) platinum planes. Further characterization of the electrodes was conducted by Scanning electron microscopy (SEM) and Microcomputed tomography (Micro-CT); the results are shown in Figures S1 and S2.

2.2. Structure and Composition

Figure 3 shows the XRD patterns of the ALD-synthesised electrodes. In the case of the 20c Pt electrode, the two reflections at 39.5° and 44.4° correspond to the platinum (111) and (200) planes. In the case of the titania-containing electrode, the reflections of platinum are broadened because of the smaller particle size. In the unmodified carbon paper, the two reflections are attributed to the (100) and (101) planes of the graphite content of the carbon fibre GDL.

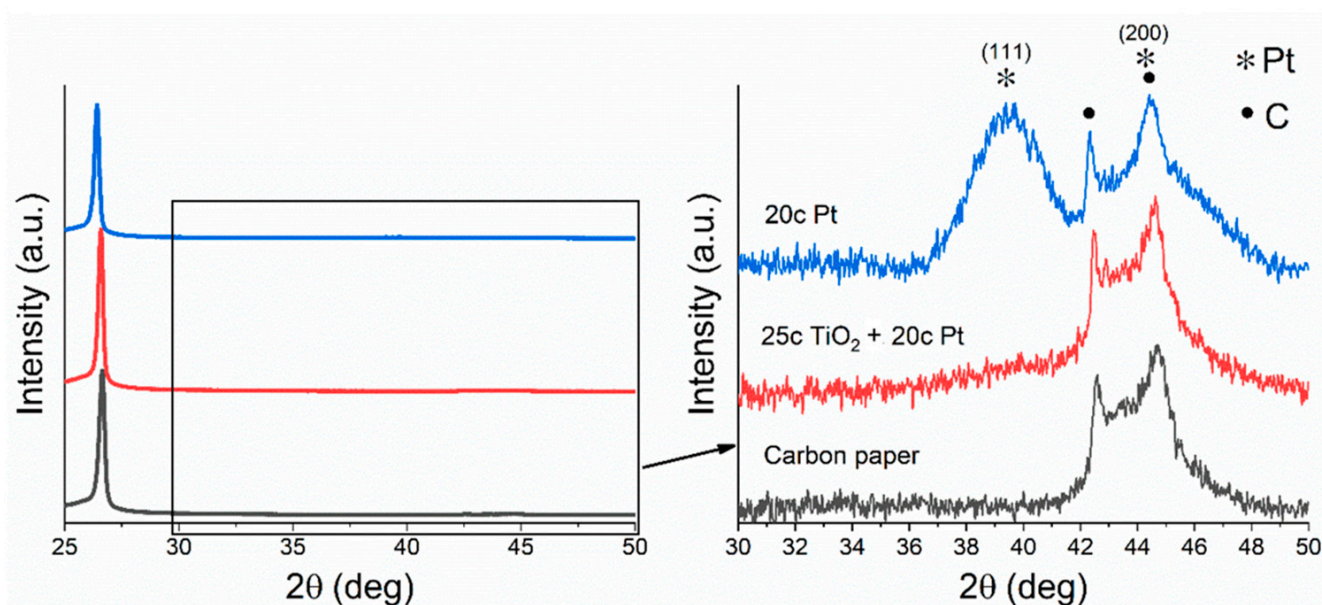


Figure 3. Characteristic XRD patterns of the ALD-synthesized electrodes.

The crystallite size calculation by the Scherrer equation was only possible in the case of the 20c Pt electrode due to the broadened reflection in the titanate-containing sample's pattern. The calculated crystallite size of 3.12 nm shows good agreement with the value obtained from the evaluation of the TEM images.

2.3. Electrocatalytic Measurements

The electrocatalytic properties of the ALD-synthesized electrodes were investigated by cyclic voltammetry (CV) in 0.5 M sulphuric acid and 0.5 M sulphuric acid/0.5 M methanol electrolytes (Figure 4). To calculate the electrochemical surface area (ECSA) of the catalyst, CV was recorded in 0.5 M sulphuric acid. The hydrogen adsorption/desorption region is visible between 0 and 0.4 V (vs. RHE) in Figure 4a. The electrochemical surface area was calculated by Equation (3) as 55.35 and 80.05 $\text{m}^2 \text{g}_{\text{Pt}}^{-1}$ for the 20c Pt and 25c $\text{TiO}_2 + 20\text{c Pt}$ catalysts, respectively.

The methanol oxidation properties of the electrodes were evaluated by measuring cyclic voltammograms in 0.5 M sulphuric acid/0.5 M methanol electrolyte. The higher the i_f/i_b ratio (i.e., the ratio of the peak current of the forward (i_f) and backward (i_b) scan), the more efficient the oxidation of methanol to CO_2 , which means less carbonaceous species accumulation on the surface of the catalyst. Manoharan and Goodenough stated that the i_b is connected to the oxidation of the CO remaining on the platinum surface, while the i_f peak is associated with freshly chemisorbed species. Consequently, the two main oxidation peaks do not share the same chemical origin. Their assessment is based on the increased i_f/i_b ratio with the increased upmost limiting potential closer to the onset potential of the OER, where more active surface oxygen species occupied the catalyst surface [24]. The i_f/i_b ratio improved from 0.69 to 0.78 between 20c Pt and 25c $\text{TiO}_2 + 20\text{c Pt}$. This indicates an improved catalytic activity of the titania-supported catalyst compared to the bare carbon supported counterpart.

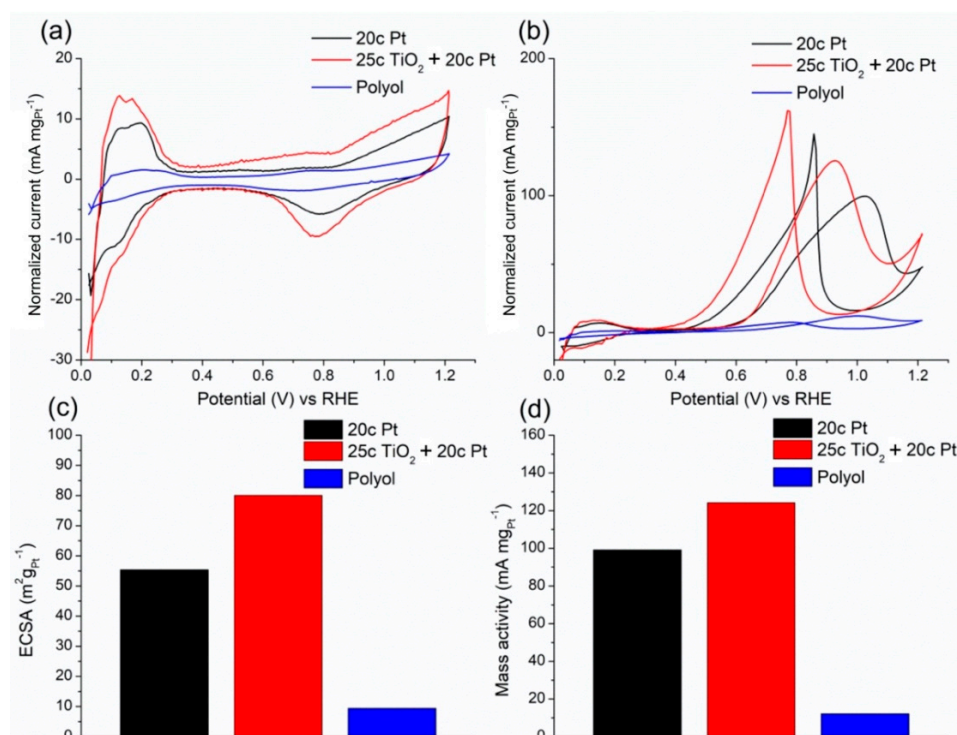


Figure 4. Cyclic voltammograms measured in 0.5 M H₂SO₄ (a) and 0.5 M methanol/0.5 M H₂SO₄ electrolytes (b), the electrochemically active surface area (c), and the mass activity (d) of the ALD-synthesised catalysts compared to the drop-casted platinum nanoparticle catalysts.

Table 1 shows the i_f/i_b ratios of similar catalysts from the literature and compares them to those obtained for our systems. It is clear that the ALD-synthesized titanium dioxide support layer improved the catalytic activity, and the obtained ratios are comparable to those reported in recent works. It should be noted here that the direct comparison between different works can be misleading since the i_f/i_b ratio can change with different scan rate [25]. It is also important to note that some publications take a different position; for example, Augusta et al. claim that the two peaks share the same chemical origin, namely, the methanol oxidation on the free Pt surface. They base this hypothesis on in situ Surface-enhanced infrared absorption spectroscopy (SEIRAS) studies of different catalysts for the MOR [26]. Although the onset potential of the i_f peak did not change significantly, the position of the peak also shifted to a more negative potential range, indicating that it takes less energy for the reaction to occur. In this case, the i_f/i_b ratio can instead be interpreted as the degree of oxophilicity [27].

Table 1. i_f/i_b ratios of various catalysts during the methanol oxidation reaction.

Catalyst	i_f/i_b	Scan Rate (mV s ⁻¹)	Reference
20c Pt	0.69	10	This work
25c TiO ₂ + 20c Pt	0.78	10	This work
Pt/TiO ₂ -C 10% TiO ₂	0.84	20	[28]
Pt/TiO ₂ -C 30% TiO ₂	0.81	20	[28]
Pt/TiO ₂ -C 60% TiO ₂	0.78	20	[28]
Pt/TiO ₂	1.21	20	[29]
Pt/CNT	0.89	20	[29]
Pt/CNT/TiO ₂	0.99	20	[29]
Pt-TiO ₂	1.88	50	[30]
Pt-C/TiO ₂	1.29	50	[30]
Pt-C	0.83	50	[30]
Pt/TiO ₂ -rGO	1.17	50	[31]

The most important benefit of the ALD method is that it utilizes the expensive platinum metal much more efficiently than wet chemical catalyst synthesis methods. This is evident from the mass activity values (Figure 4d), which were found to be significantly higher in ALD catalysts than in the polyol-based reference material. The mass activity of the 20c Pt electrode was 99.3 mA mg^{-1} , while in the case of the titanate-containing catalyst it was 125.7 mA mg^{-1} . Although it was previously reported that the mass activity decreases with decreasing particle size, we found the opposite tendency below 4.5 nm [23]. We assume that despite the smaller size, the increased mass activity can be linked to TiO_2 . Deng et al. found changes in the electronic structure of Pt after it was deposited on a TiO_2 -containing catalyst. This can be linked to strong metal–support interactions, which can ultimately cause the weakening of Pt–CO bonds [22]. However, this phenomenon needs further investigation.

To test the practical applicability and long-term stability of the electrodes, chronoamperometric tests were executed. The three electrodes are compared in Figure S4. It is clearly visible that the normalized current in the case of the 25c TiO_2 + 20c Pt catalyst decreased more slowly over time and reached the minimum later than for platinum-only electrodes.

In summary, the combination of ALD-synthesized Pt and TiO_2 resulted in a promising new, carbon-paper-based, binder-free anode catalyst that offers one order of magnitude better mass activity than its wet-chemistry-derived counterparts while maintaining a comparable CO poisoning tolerance.

3. Materials and Methods

Working electrodes were synthesized by atomic layer deposition, depositing a titanium dioxide layer and platinum nanoparticles on AvCarb P75 carbon paper (Lowell, MA, USA) support. The high aspect ratio (HAR) chamber of the Beneq TFS200 ALD (Espoo, Finland) equipment was used during the process. In the case of TiO_2 , the two precursors were titanium tetrachloride (TiCl_4) (PURATREM Alfa Aesar, 99.0%) (Haverhill, MA, USA) and water (Milli-Q) (Darmstadt, Germany), while in the case of platinum the precursors were trimethyl(methylcyclopentadienyl)-platinum (IV) (MeCpPtMe_3) (Strem Chemicals, Inc. 99% (99.999%-Pt)) (Kehl, Germany) and oxygen (O_2) (Messer 5.0) (Szeged, Hungary). Each synthesis was executed with 10 s of precursor residence time and 20 s of purging by N_2 gas between two precursor introductions. To prepare the electrode, first 25 cycles of TiO_2 , then 20 cycles of platinum were deposited on the same GDL (25c TiO_2 + 20c Pt). For comparison, we also prepared carbon paper/Pt nanoparticle electrodes without the underlying titanium dioxide layer (20c Pt). Before and after the synthesis, the weight of the carbon paper was measured to calculate the weight of the deposited catalysts. The TiO_2 loading was 0.019 mg cm^{-2} , while the platinum loadings were 0.277 and 0.116 mg cm^{-2} in 20c Pt and 20c Pt + 25c TiO_2 catalysts, respectively. The lower Pt loading in the titania-containing electrode can be attributed to the higher surface energy of TiO_2 . We also prepared electrodes by drop-casting platinum nanoparticles prepared by the traditional polyol method on AvCarb P75 carbon paper. The average size of the used nanoparticles was $4.4 \pm 0.7 \text{ nm}$.

3.1. Catalyst/Electrode Characterisation

The as-synthesized catalysts were characterized by transmission electron microscopy. A FEI Tecnai G² 20 X-Twin microscope (Hillsboro, OR, USA) was operated at 200 kV accelerating voltage. The samples were prepared as follows: a small portion of the electrode was sonicated in isopropanol for 10 min, and a portion of the obtained suspension was drop-casted on a TEM grid and then examined. The surface structure of the electrodes was studied by scanning electron microscopy (SEM) using a Thermo Fisher Scientific Apreo C instrument (Waltham, MA, USA). The crystal structure of the electrodes was analysed by powder X-ray diffraction (XRD) measurements. The $\text{Cu K}\alpha$ radiation was generated by a Philips PW1830 X-ray generator (Amsterdam, Netherlands) operating at 40 kV and 30 mA,

at a scan speed of 5 s step^{-1} (0.02°). The crystallite size of the catalyst was calculated using the Scherrer equation:

$$D = K\lambda / \beta \cos \theta \quad (1)$$

where D is the crystallite size, K is a constant related to crystallite shape usually taken as 0.9, λ is the X-ray wavelength in nanometres, β is the peak width at half maximum height in radians, and θ is the position of the peak [32]. The homogeneity of the catalyst coverage was examined by a Bruker Skyscan 2211 micro-CT (Billerica, MA, USA) unit.

3.2. Electrochemical Measurements

Electrochemical measurements were conducted in a custom-made three-electrode PTFE cell using an ACM Instruments Gill AC electrochemical workstation (Grange-over-Sands, UK) at room temperature (23°C). ALD-modified AvCarb P75 carbon papers were used as working electrodes, while Ag/AgCl (3 M NaCl) and Pt wire were utilized as reference and counter electrodes, respectively. The two halves of the cell were separated by a glass frit. During the measurements 0.5 M sulphuric acid and 0.5 M sulphuric acid + 0.5 M methanol were used as electrolytes. The measured potentials (V vs. Ag/AgCl 3 M NaCl) were converted to the reversible hydrogen electrode scale by the following equation:

$$E(\text{vs. RHE}) = E + E(\text{vs. Ag/AgCl}) + 0.059\text{pH} \quad (2)$$

where E is the experimentally measured potential vs. Ag/AgCl and $E_{\text{Ag/AgCl}}$ (vs. SHE) = 0.195 V at room temperature (25°C). The electrochemical properties of the ALD-modified electrodes were examined by cyclic voltammetry between 0 and 1200 mV vs. RHE at a sweep rate of 10 mV s^{-1} . The electrochemical surface area (ECSA) of the catalysts was calculated from the hydrogen adsorption/desorption region of the obtained voltammograms by the following equation:

$$\text{ECSA} \left(\text{m}^2 \text{g}_{\text{Pt}}^{-1} \right) = \frac{Q_{\text{h}} \left(\text{mC cm}^{-2} \right)}{0.21 \left(\text{mC cm}^{-2} \right) * W_{\text{Pt}} \left(\text{mg}_{\text{Pt}} \text{cm}^{-2} \right)} * 10^{-1} \quad (3)$$

where Q_{h} is the charge calculated from the H_{des} region of the voltammogram, 0.21 represents a charge required to oxidize a monolayer of hydrogen adsorbed on Pt, and W_{Pt} is the loading of platinum [33–35]. The methanol oxidising properties and the CO tolerance of the electrode were evaluated from the CV measured in the methanol-containing electrolyte by comparing the ratio of the peak current during the forward (i_{f}) and the backward (i_{b}) scan. It is generally accepted that the ratio of these peaks is correlated with the tolerance of the catalyst to carbonaceous species. An increase in the $i_{\text{f}}/i_{\text{b}}$ ratio implies enhanced CO oxidation properties of the catalyst [36].

Chronoamperometric measurements were performed to investigate the long-term stability of our electrodes: 4000 s at the potential of 1 V vs. RHE in the same 3-electrode cell containing 0.5 M methanol and 0.5 M H_2SO_4 electrolyte.

4. Conclusions

Our results suggest that atomic layer deposition is a suitable method to prepare well-distributed platinum nanoparticles on carbon paper and TiO_2 -covered carbon paper supports, where both the platinum and TiO_2 are synthesised directly by ALD and deposited without using any binder. The morphology and the crystal structure of the as-prepared electrodes were characterised and the electrocatalytic methanol oxidation activity was assessed using cyclic voltammetry. The ALD method makes creating very small nanoparticles with well-controlled, narrow particle size distribution feasible. This yielded platinum nanoparticles with high electrochemical surface area and mass activity on titania-covered carbon paper GDL support. The mass activity of the new catalyst exceeded that of the reference Pt catalyst obtained by traditional wet chemistry by one order of magnitude. Moreover, the increased $i_{\text{f}}/i_{\text{b}}$ ratio implies better methanol oxidation properties and renders the reported

preparation method a promising alternative for creating poisoning-tolerant anode catalysts in direct methanol fuel cells.

Supplementary Materials: The following are available online at <https://www.mdpi.com/2073-4344/11/2/154/s1>, Figure S1: Scanning electron microscopy images of the surfaces of the ALD-prepared electrodes. The images in the left column were generated made by the secondary electron (SE) technique and the images on the right by the backscattered electron (BSE) technique. (a,b) 20c Pt; (c,d) 25c TiO₂ + 20c Pt; (e,f) bare carbon paper; Figure S2: Micro-CT images of the bare AvCarb P75 carbon paper (A), the 20c Pt electrode (B), the 25c TiO₂ + 20c Pt electrode (C), and side view of the 20c Pt electrode (D); Figure S3: Transmission electron microscopic image (a) and electron diffractogram (b) of the polyol catalyst; Figure S4: Chronoamperometric measurements of the ALD-prepared catalysts: 25c TiO₂ + 20c Pt (a); 20c Pt (b); Polyol catalyst (c).

Author Contributions: Conceptualization G.B. performed the synthesis of the electrodes, evaluated the results and drafted the manuscript. T.G. performed the electrochemical measurements. H.H. contributed to the design of the project, assisted in the evaluation of the results, and contributed to drafting the manuscript. L.V. performed the Micro-CT measurements and contributed to evaluating the data. I.S. performed the Scanning electron microscopic measurements and contributed to evaluating the data. D.S. performed the XRD measurements and contributed to evaluating the data. Z.K. supervised the project. Á.K. founded and supervised the project, revised the manuscript. All authors have read and agreed to the published version of the manuscript.

Funding: This research was funded by the Hungarian National Research, Development and Innovation Office, grant number GINOP-2.3.3-15-2016-00010. D.S. acknowledges the support of the János Bolyai Research Scholarship of the Hungarian Academy of Sciences.

Data Availability Statement: The data presented in this study are available on request from the corresponding author.

Conflicts of Interest: The authors declare no conflict of interest.

References

1. Ong, B.C.; Kamarudin, S.K.; Basri, S. Direct liquid fuel cells: A review. *Int. J. Hydrog. Energy* **2017**, *42*, 10142–10157. [[CrossRef](#)]
2. Saurat, M.; Bringezu, S. Platinum group metal flows of Europe, part I: Global supply, use in industry, and shifting of environmental impacts. *J. Ind. Ecol.* **2008**, *12*, 754–767. [[CrossRef](#)]
3. Chrzanowski, W.; Wieckowski, A. Surface structure effects in platinum/ruthenium methanol oxidation electrocatalysis. *Langmuir* **1998**, *14*, 1967–1970. [[CrossRef](#)]
4. Kadirgan, F.; Beden, B.; Leger, J.M.; Lamy, C. Synergistic effect in the electrocatalytic oxidation of methanol on platinum+palladium alloy electrodes. *J. Electroanal. Chem. Interfacial Electrochem.* **1981**, *125*, 89–103. [[CrossRef](#)]
5. Xu, J.; Liu, X.; Chen, Y.; Zhou, Y.; Lu, T.; Tang, Y. Platinum-Cobalt alloy networks for methanol oxidation electrocatalysis. *J. Mater. Chem.* **2012**, *22*, 23659–23667. [[CrossRef](#)]
6. Zaidi, S.M.J.; Rauf, M.A. *Fuel Cell Fundamentals*; Wiley: Hoboken, NJ, USA, 2009; ISBN 9780387735313.
7. Hua, H.; Hu, C.; Zha, Z.; Liu, H.; Xie, X.; Xi, Y. Pt nanoparticles supported on submicrometer-sized TiO₂ spheres for effective methanol and ethanol oxidation. *Electrochim. Acta* **2013**, *105*, 130–136. [[CrossRef](#)]
8. Wang, Y.; Mohamedi, M. Hierarchically organized nanostructured TiO₂/Pt on microfibrillar carbon paper substrate for ethanol fuel cell reaction. *Int. J. Hydrog. Energy* **2017**, *42*, 22796–22804. [[CrossRef](#)]
9. Abdullah, N.; Kamarudin, S.K. Titanium dioxide in fuel cell technology: An overview. *J. Power Sources* **2015**, *278*, 109–118. [[CrossRef](#)]
10. Lasch, K.; Jörissen, L.; Garcke, J. Effect of metal oxides as co-catalysts for the electro-oxidation of methanol on platinum-ruthenium. *J. Power Sources* **1999**, *84*, 225–230. [[CrossRef](#)]
11. Stepanov, A.L.; Golubev, A.N.; Nikitin, S.I.; Osin, Y.N. A review on the fabrication and properties of platinum nanoparticles. *Rev. Adv. Mater. Sci.* **2014**, *38*, 160–175.
12. Islam, M.A.; Bhuiya, M.A.K.; Islam, M.S. A Review on Chemical Synthesis Process of Platinum Nanoparticles. *Asia Pac. J. Energy Environ.* **2014**, *1*, 101–114. [[CrossRef](#)]
13. Bodner, M.; García, H.R.; Steenberg, T.; Terkelsen, C.; Alfaro, S.M.; Avcioglu, G.S.; Vassiliev, A.; Primdahl, S.; Hjuler, H.A. Enabling industrial production of electrodes by use of slot-die coating for HT-PEM fuel cells. *Int. J. Hydrog. Energy* **2019**, *44*, 12793–12801. [[CrossRef](#)]
14. Morgan, R.D.; Haan, J.L.; Masel, R.I. Effects of Nafion loading in anode catalyst inks on the miniature direct formic acid fuel cell. *J. Power Sources* **2010**, *195*, 6405–6410. [[CrossRef](#)]

15. Sasikumar, G.; Ihm, J.W.; Ryu, H. Optimum Nafion content in PEM fuel cell electrodes. *Electrochim. Acta* **2004**, *50*, 601–605. [[CrossRef](#)]
16. Tu, H.C.; Wang, W.L.; Wan, C.C.; Wang, Y.Y. Novel method for the synthesis of hydrophobic Pt-Ru nanoparticles and its application to preparing a Nafion-free anode for the direct methanol fuel cell. *J. Phys. Chem. B* **2006**, *110*, 15988–15993. [[CrossRef](#)]
17. Xu, H.; Reunchan, P.; Ouyang, S.; Tong, H.; Umezawa, N.; Kako, T.; Ye, J. Anatase TiO₂ single crystals exposed with high-reactive {111} facets toward efficient H₂ evolution. *Chem. Mater.* **2013**, *25*, 405–411. [[CrossRef](#)]
18. Cheng, N.; Shao, Y.; Liu, J.; Sun, X. Electrocatalysts by atomic layer deposition for fuel cell applications. *Nano Energy* **2016**, *29*, 220–242. [[CrossRef](#)]
19. Yan, H.; Cheng, H.; Yi, H.; Lin, Y.; Yao, T.; Wang, C.; Li, J.; Wei, S.; Lu, J. Single-Atom Pd1/Graphene Catalyst Achieved by Atomic Layer Deposition: Remarkable Performance in Selective Hydrogenation of 1,3-Butadiene. *J. Am. Chem. Soc.* **2015**, *137*, 10484–10487. [[CrossRef](#)]
20. Gould, T.D.; Lubers, A.M.; Corpuz, A.R.; Weimer, A.W.; Falconer, J.L.; Medlin, J.W. Controlling nanoscale properties of supported platinum catalysts through atomic layer deposition. *ACS Catal.* **2015**, *5*, 1344–1352. [[CrossRef](#)]
21. Yang, H.; Chen, Y.; Qin, Y. Application of atomic layer deposition in fabricating high-efficiency electrocatalysts. *Chin. J. Catal.* **2020**, *41*, 227–241. [[CrossRef](#)]
22. Deng, J.; Zhang, J.; Chen, J.; Luo, Y.; Chen, Y.; Xue, Y.; Wang, G.; Wang, R. Fabrication of layered porous TiO₂/carbon fiber paper decorated by Pt nanoparticles using atomic layer deposition for efficient methanol electro-oxidation. *J. Electroanal. Chem.* **2020**, *148*, 114468. [[CrossRef](#)]
23. Frelink, T.; Visscher, W.; van Veen, J.A.R. Particle size effect of carbon-supported platinum catalysts for the electrooxidation of methanol. *J. Electroanal. Chem.* **1995**, *382*, 65–72. [[CrossRef](#)]
24. Manoharan, R.; Goodenough, J.B. Methanol oxidation in acid on ordered NiTi. *J. Mater. Chem.* **1992**, *2*, 875–887. [[CrossRef](#)]
25. Te Hsieh, C.; Tzou, D.Y.; Jiang, M.T. Methanol electro-oxidation on Pt nanocatalysts prepared by atomic layer deposition. *J. Electroanal. Chem.* **2017**, *794*, 139–147. [[CrossRef](#)]
26. Hofstead-Duffy, A.M.; Chen, D.J.; Sun, S.G.; Tong, Y.J. Origin of the current peak of negative scan in the cyclic voltammetry of methanol electro-oxidation on Pt-based electrocatalysts: A revisit to the current ratio criterion. *J. Mater. Chem.* **2012**, *22*, 5205–5208. [[CrossRef](#)]
27. Chung, D.Y.; Lee, K.J.; Sung, Y.E. Methanol electro-oxidation on the Pt surface: Revisiting the cyclic voltammetry interpretation. *J. Phys. Chem. C* **2016**, *120*, 9028–9035. [[CrossRef](#)]
28. Kuriganova, A.B.; Leontyev, I.N.; Alexandrin, A.S.; Maslova, O.A.; Rakhmatullin, A.I.; Smirnova, N.V. Electrochemically synthesized Pt/TiO₂-C catalysts for direct methanol fuel cell applications. *Mendeleev Commun.* **2017**, *27*, 67–69. [[CrossRef](#)]
29. Bedolla-Valdez, Z.I.; Verde-Gómez, Y.; Valenzuela-Muñiz, A.M.; Gochi-Ponce, Y.; Oropeza-Guzmán, M.T.; Berhault, G.; Alonso-Núñez, G. Sonochemical synthesis and characterization of Pt/CNT, Pt/TiO₂, and Pt/CNT/TiO₂ electrocatalysts for methanol electro-oxidation. *Electrochim. Acta* **2015**, *186*, 76–84. [[CrossRef](#)]
30. Wu, X.; Zhuang, W.; Lu, L.; Li, L.; Zhu, J.; Mu, L.; Li, W.; Zhu, Y.; Lu, X. Excellent performance of Pt-C/TiO₂ for methanol oxidation: Contribution of mesopores and partially coated carbon. *Appl. Surf. Sci.* **2017**, *426*, 890–896. [[CrossRef](#)]
31. Zhuang, W.; He, L.; Zhu, J.; An, R.; Wu, X.; Mu, L.; Lu, X.; Lu, L.; Liu, X.; Ying, H. TiO₂ nanofibers heterogeneously wrapped with reduced graphene oxide as efficient Pt electrocatalyst supports for methanol oxidation. *Int. J. Hydrog. Energy* **2015**, *40*, 3679–3688. [[CrossRef](#)]
32. Monshi, A.; Foroughi, M.R.; Monshi, M.R. Modified Scherrer Equation to Estimate More Accurately Nano-Crystallite Size Using XRD. *World J. Nano Sci. Eng.* **2012**, *2*, 154–160. [[CrossRef](#)]
33. Chaiburi, C.; Hacker, V. Catalytic activity of various platinum loading in acid electrolyte at 303 K. *Energy Procedia* **2017**, *138*, 229–234. [[CrossRef](#)]
34. Pozio, A.; De Francesco, M.; Cemmi, A.; Cardellini, F.; Giorgi, L. Comparison of high surface Pt/C catalysts by cyclic voltammetry. *J. Power Sources* **2002**, *105*, 13–19. [[CrossRef](#)]
35. Trasatti, S.; Petrii, O.A. International Union of Pure and Applied Chemistry Physical Chemistry Division Commission on Electrochemistry: Real Surface Area Measurements in Electrochemistry. *Pure Appl. Chem.* **1991**, *63*, 711–734. [[CrossRef](#)]
36. Sarma, L.S.; Taufany, F.; Hwang, B.J. Electrocatalyst Characterization and Activity Validation—Fundamentals and Methods. In *Electrocatalysis of Direct Methanol Fuel Cells: From Fundamentals to Applications*; Wiley: Hoboken, NJ, USA, 2009; pp. 115–163. [[CrossRef](#)]